Ablation and transmission of thin solid targets irradiated by intense extreme ultraviolet laser radiation

V. Aslanyan, I. Kuznetsov, H. Bravo, M. R. Woolston, A. K. Rossall, C. S. Menoni, J. J. Rocca, and G. J. Tallents

Citation: APL Photonics **1**, 066101 (2016); doi: 10.1063/1.4953669
View online: http://dx.doi.org/10.1063/1.4953669
View Table of Contents: http://aip.scitation.org/toc/app/1/6
Published by the American Institute of Physics

Ablation and transmission of thin solid targets irradiated by intense extreme ultraviolet laser radiation

V. Aslanyan,[1] I. Kuznetsov,[2] H. Bravo,[2] M. R. Woolston,[2] A. K. Rossall,[1]
C. S. Menoni,[2] J. J. Rocca,[2,3] and G. J. Tallents[1]
[1]*York Plasma Institute, University of York, York, Heslington YO10 5DQ, United Kingdom*
[2]*Department of Electrical and Computer Engineering, Colorado State University, Fort Collins, Colorado 80523, USA*
[3]*Department of Physics, Colorado State University, Fort Collins, Colorado 80523, USA*

(Received 1 April 2016; accepted 30 May 2016; published online 12 July 2016)

The interaction of an extreme ultraviolet (EUV) laser beam with a parylene foil was studied by experiments and simulation. A single EUV laser pulse of nanosecond duration focused to an intensity of 3×10^{10} W cm^{-2} perforated micrometer thick targets. The same laser pulse was simultaneously used to diagnose the interaction by a transmission measurement. A combination of 2-dimensional radiation-hydrodynamic and diffraction calculations was used to model the ablation, leading to good agreement with experiment. This theoretical approach allows predictive modelling of the interaction with matter of intense EUV beams over a broad range of parameters. [http://dx.doi.org/10.1063/1.4953669]

I. INTRODUCTION

The interactions of intense laser beams with matter have been the subject of active study since the invention of the laser.[1,2] They are of great importance to fundamental science as well as for numerous applications. More recently, the development of intense sources of extreme ultraviolet (EUV)/soft x-ray radiation has motivated interest in the study of laser-plasma interactions at short wavelengths.[3–9] We consider in this paper the interaction of table-top, high repetition rate EUV/soft x-ray lasers[10–13] with solid targets. Such lasers can enable fundamental studies and be utilized for applications such as nanomachining[14,15] and the development of nanoprobes.[16–18]

We present the results of experiments undertaken with an argon capillary discharge laser, producing nanosecond pulses at a wavelength of 46.9 nm, focused onto thin parylene-N targets. This type of plastic contains equal proportions of hydrogen and carbon, which simplifies radiation-hydrodynamic simulations. Two target thicknesses, 429 and 1028 nm, were chosen so that a single laser pulse of 50 μJ could penetrate and be partially transmitted through the targets. Measuring the laser beam transmission through the targets enables a measure of the target ablation unaffected by late time target shock damage, as the unablated target material is opaque to the laser radiation. We have used spherical multilayer mirrors to focus the laser so as to increase the focused irradiance to above 10^{10} W cm^{-2}.

II. EXPERIMENTAL SETUP

In order to maximise the peak intensity and total energy delivered to the target, the EUV laser beam was focused by a single spherical Sc/Si multilayer mirror (M1) with a relatively short focal length of 50 mm. A second identical mirror (M2) recollimated the beam, so that it could be measured by a back-thinned CCD camera after attenuation by an aluminum filter. This experimental setup, shown in Figure 1, required that the mirrors be placed at a relatively large tilt angle $\alpha = 4.7°$, leading to aberration; simulations of the resultant focal spots are presented in Sec. III.

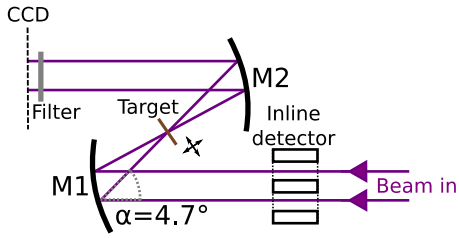

FIG. 1. Experimental setup used to ablate thin targets using focused EUV laser light ($\lambda = 46.9$ nm) and measure the transmitted portion of the beam by a CCD. The inline photoionization detector is used to measure shot energies.

The laser operates at a wavelength $\lambda = 46.9$ nm and outputs pulses with a duration of 1.1 ± 0.1 ns and energy of 50 ± 5 μJ. As the laser beam passes through an inline detector, photoionization of the residual gas in the vacuum chamber is measured with an accuracy of 10% to give a value for the pulse energy after initial calibration with a gold photodiode. The energy response of the photodiode is known *a priori*; after calibration, the background pressure and position of the beam relative to the inline detector were held constant. These measurements provide accurate intensity values, as required by radiation-hydrodynamic codes, regardless of the shot-to-shot beam energy variation. An XYZ translation stage allowed scans to be made in the target position along the beam axis, as well as to a fresh target as required. The target thickness was characterised by white light interferometry.[19]

III. FOCAL SPOT SIMULATIONS

The intensity profile at the targets was simulated by solving a Fresnel diffraction integral. The incident laser beam profile was measured by the CCD, at a position before the experimental setup. The properties of the multilayer mirrors were simulated by the IMD code[20] for a range of angles of ray incidence upon the mirror. A combination of both of these results, together with the surface geometry of the mirror, was input into a code solving the diffraction integral on a series of planes at various distances close to the focal length of the mirror. The targets were positioned at one focal length from the mirror with an accuracy of 0.5 mm; comparisons of the simulated intensity profile to micrographs of the perforations allowed the precise target distance to be determined.

The beam created by capillary discharge lasers typically has an annular profile, which diverges spherically from the end of the capillary. This type of beam profile is common to capillary discharge lasers, arising from beam refraction along the plasma column caused by a convex radial profile of the refractive index in the gain medium that has its maximum electron density on axis.[21] A fit to measurements of the beam profile yields an analytic pseudo-Gaussian function of the form

$$I(r) = (A - c)\exp\left(-\frac{(r - r_0)^2}{w^2}\right) + c, \qquad r \le r_0, \tag{1}$$

$$I(r) = A\exp\left(-\frac{(r - r_0)^2}{w^2}\right), \qquad r > r_0, \tag{2}$$

where r is the radial distance from the centre of the beam profile and A, c, r_0, and w are fit parameters.

In order to simulate the asymmetric intensity profile close to the focal plane of the tilted multilayer mirror M1, we have solved the Fresnel diffraction integral.[22] In polar coordinates it is given by

$$\tilde{u}(\tilde{r},\tilde{\theta}) = \mathcal{N}\int_0^{2\pi}\int_0^{\infty} u(r,\theta)\frac{\exp(ik\rho)}{\rho^2} r\,dr\,d\theta, \tag{3}$$

where the wavenumber $k = 2\pi/\lambda$, u is the incident wave amplitude at radial position r and azimuthal angle θ, $\tilde{u}$, $\tilde{r}$, and $\tilde{\theta}$ are the corresponding quantities at a distance z along the optical axis, ρ is the geometrical distance between points at r,θ and $\tilde{r},\tilde{\theta}$, and $\mathcal{N}$ is a normalization factor. The diffracted intensity is given by $I(\tilde{r},\tilde{\theta}) = P|\tilde{u}(\tilde{r},\tilde{\theta})|^2$, where P is the total instantaneous power of in the beam.

Light travelling along the z-axis reflected from a curved optic, whose surface is given by an analytical function $h = h(r,\theta)$, acquires a geometric phase $\phi_G = \exp(-2ikh)$. For a spherical mirror with radius of curvature R_c, tilted by an angle α along a line of $\theta = 0$, the surface is given by

$$h_{SM} = \sqrt{R_c^2 \cos^2\alpha - r^2 + 2R_c r \cos\theta \sin\alpha}. \tag{4}$$

A general two-dimensional surface h makes an angle η with the z-axis which satisfies

$$\tan(\eta) = \sqrt{\left(\frac{\partial h}{\partial r}\right)^2 + \frac{1}{r^2}\left(\frac{\partial h}{\partial \theta}\right)^2}. \tag{5}$$

Therefore, η can be taken as the incidence angle of collimated rays on the optic. This is an important consideration for multilayer mirrors, because both the reflectivity and reflected phase are often strongly dependent on the angle of incidence. We have simulated these two properties of the Sc/Si mirrors with the IMD code,[20] which calculates the interference of rays reflected and transmitted at the interfaces of each dielectric layer. The results of IMD are parameterised with analytic functions by curve fitting, to be used in the numerical solver of the Fresnel integral. The multilayer phase is approximately quadratic, given by

$$\phi_{MLM} = \exp(iA_\phi \eta^2), \tag{6}$$

where A_ϕ is a fit parameter. The reflectance $\mathbb{r}$, used in diffraction calculations and related to the reflectivity by $\mathbb{R} = |\mathbb{r}|^2$, may be approximated by a modified hyperbolic tangent function,

$$\mathbb{r} = A_\mathbb{r}(1 + D\eta^2)\{1 - \tanh[C(|\eta| - B)]\}, \tag{7}$$

where $A_\mathbb{r}$, B, C, D are the fit parameters. These analytic fits are compared to the IMD simulation in Figure 2 and perform well for the range of incidence angles, $|\eta| < 10°$, in this experiment.

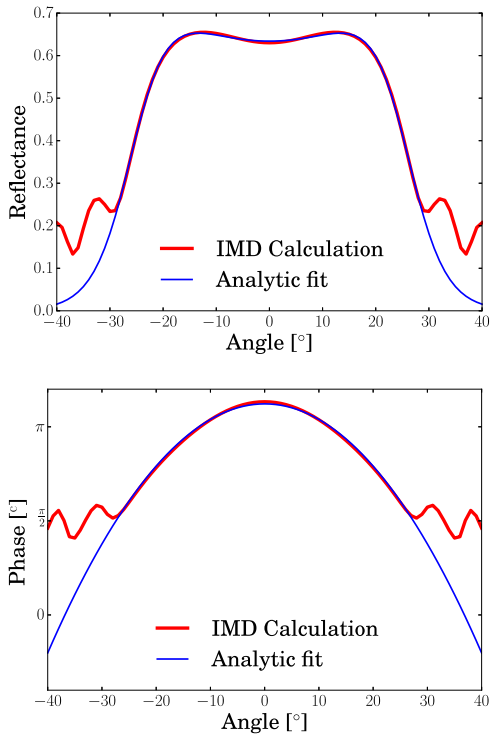

FIG. 2. The angle-dependent reflectance and phase of a Sc/Si multilayer mirror used for the experiments described here, simulated by the IMD code and approximated by analytic functions.

We have solved the Fresnel diffraction integral of Eq. (3) for the capillary laser's beam profile reflected by the tilted multilayer mirror by a Newton-Cotes method.[23] Taking the incident wave amplitude $u = \phi_G \phi_{MLM} \mathbb{r} \sqrt{I}$ on a grid of coordinates r, θ incorporates the beam profile, tilt, and multilayer effects. A high degree of parallelism was achieved in the CPU code by decomposing the domain of output coordinates $\tilde{r}$ and $\tilde{\theta}$. The results are normalised to the measured laser pulse energy. The intensity profile for a 50 μJ pulse focused under experimental conditions is shown in Figure 3(a).

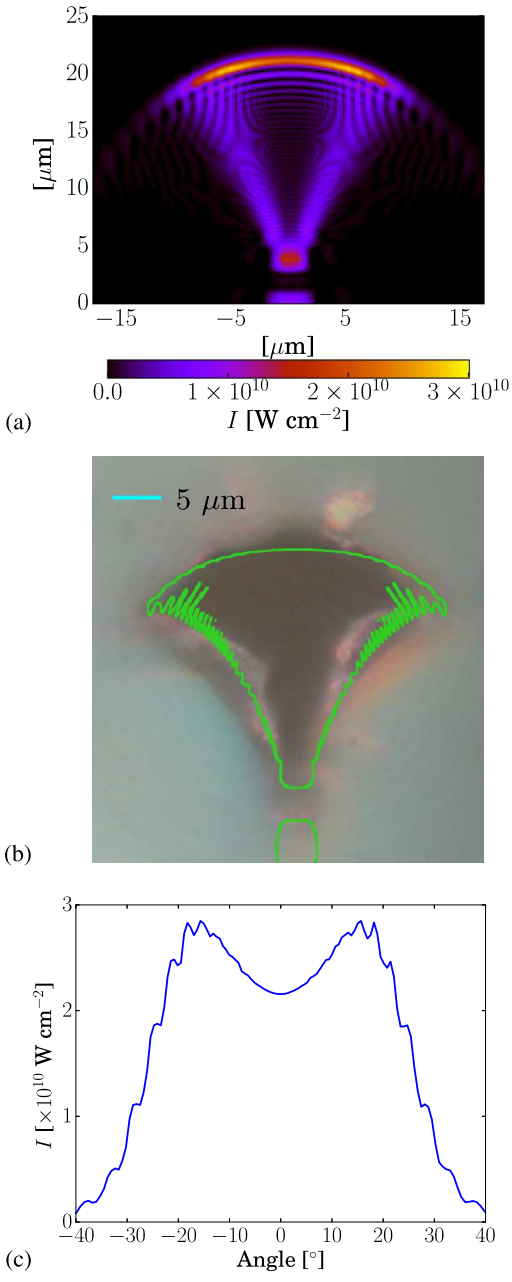

FIG. 3. (a) Simulated peak intensity profile at a distance of 49.75 mm from a Sc/Si multilayer mirror ($f = 50$ mm) tilted by an angle $\alpha = 4.7°$ and a laser pulse energy of 50 μJ. (b) Contours corresponding to 5% of peak intensity from this profile overlaid onto a micrograph of a 1028 nm thick parylene target after 30 shots. (c) Intensity variation along the upper circular arc of the intensity profile as a function of the angle to the vertical of the page.

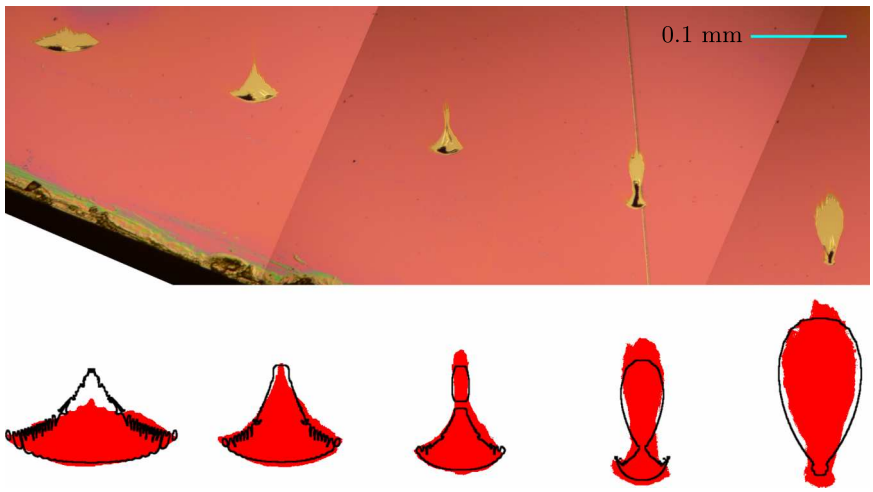

FIG. 4. (Top) Micrograph of ablation profiles after >100 shots of parylene coated onto glass slides; adjacent spots were exposed 0.1 mm apart along the beam propagation axis, with the right-most spot separated from the mirror by a single focal length. The blackened regions correspond to ablation of the glass substrate. (Bottom) The ablation profiles (red) with a constant intensity contour (black) taken from simulations.

In order to validate the diffraction calculations, we have compared contours of constant intensity to micrographs of ablation spots created by the focused laser beam; an example is shown in Figure 3(b). The contours are selected at 5% of the maximum intensity, which is consistent with detectable ablation occurring when the intensity exceeds 10^9 W cm^{-2}. The interaction of a single shot with a fresh target requires detailed radiation-hydrodynamic simulations, as outlined in Sec. IV, to match experiment. However, after a large number of shots, all regions where the intensity exceeds the ablation limit are clearly distinguishable. We have performed a scan of ablation profiles of parylene coated onto glass slides at equally spaced points along the beam propagation axis. Micrographs of the irradiated regions are shown and compared to contours of constant intensity from corresponding simulations in Figure 4. We see a good agreement between the simulations and both the perforation of the thin targets and ablation of the film coating.

IV. TARGET HYDRODYNAMICS

We have simulated target ablation and the expansion of plasma created by absorption of the focused EUV laser beam using the 2-dimensional radiation-hydrodynamic code POLLUX.[24] The code incorporates a comprehensive equation of state model, with relevant phase transitions. For plasmas, the distribution of ions is modelled by local thermodynamic equilibrium (LTE) including ionization potential depression and used to calculate the opacity due to photoionization and inverse bremsstrahlung.[25,26]

Ablation of solid-density material by EUV radiation creates a low-density plume of plasma expanding in the direction of the laser and (more slowly) laterally. For intensities considered in this paper, the plasma density drops approximately exponentially along the laser axis. The peak electron temperature $k_B T_e \simeq 5$ eV occurs close to the ablation front. At times before ablation through the target, the EUV transmission is zero, rising when the plasma is ionized to C^{2+} where the ionization potential of 47.9 eV is above the photon energy.

POLLUX allows the ablation surface, i.e., the depth below which material remains solid, to be temporally resolved. The cylindrically symmetric results for focal profiles with different peak intensities, but identical spatial extent of 2 μm and temporal duration of 1 ns, are shown in Figure 5.

Due to the asymmetry of the focal intensity profile, POLLUX cannot be used to directly simulate the 3-dimensional laser-plasma interaction. However, to obtain a 3-dimensional depth profile, the calculated ablation surfaces for a given intensity may be applied locally, because the dynamics

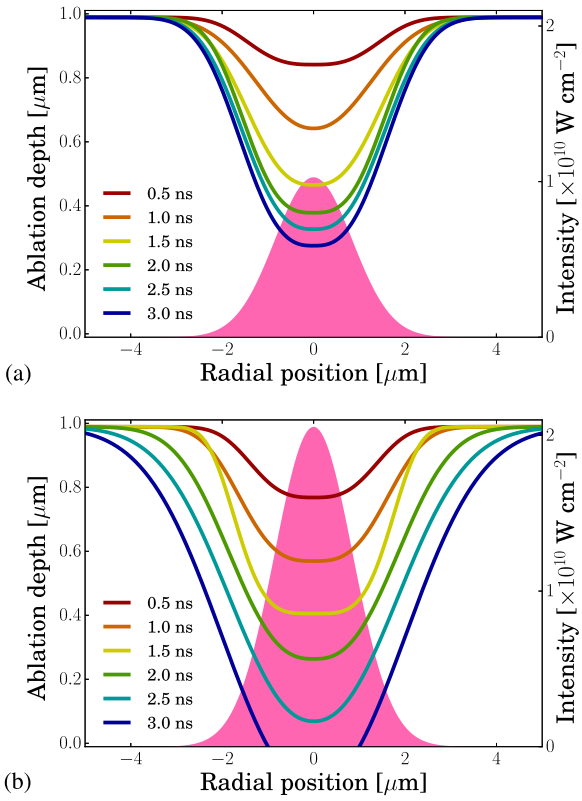

FIG. 5. Time-resolved ablation of 1028 nm thick parylene targets by incident laser radiation with a peak intensity of (a) 10^{10} W cm^{-2} and (b) 2×10^{10} W cm^{-2} and FWHM of 2 μm, as shown schematically by the shaded region. The laser pulse is temporally Gaussian with FWHM of 1 ns and the start of the simulation ($t = 0$) is taken at 1 ns before the peak of the pulse.

are characterized by low heat transport perpendicular to the beam axis. The focal intensity profiles may be decomposed into several elementary geometric components; for example, a prominent circular arc and a V-shape constitute the profile in Figure 3(a). The intensity along the arc is given in Figure 3(c), while the intensity within the V-shape makes only small departures from 5×10^9 W cm^{-2}. Taking the intensity at each point on these geometric components, we impose the appropriate ablation surface (examples of which are given in Figure 5) along a line perpendicular to the component. This approach allows a time-dependent 3-dimensional ablation depth to be calculated, as shown in Figure 6.

A contour corresponding to a zero depth describes the shape of the resultant perforation in the target that can readily be compared to targets seen in experiment. We have overlaid contours for simulations after 1, 2, and 30 shots on target onto appropriate micrographs in Figure 7. Perforation contours agree well with experiment for 2 and 30 shots, where all regions with significant incident intensity have been ablated. In both these cases, a central region with low incident intensity has been cut from the target. The agreement is worse for a single shot, where the perforation does not completely surround this central region. Stresses appear to have made this region of foil fold inwards, as seen in Figure 7(a).

V. TRANSMISSION THROUGH TARGETS

The second spherical multilayer mirror M2 was positioned one focal length (f = 50 mm) beyond the target, allowing part of the laser pulse to be transmitted when regions of the target became transparent. Generically, coherent radiation acquires an amplitude and phase modulation when interacting with matter in its focal plane. Thereafter, the beam expands laterally, making valid

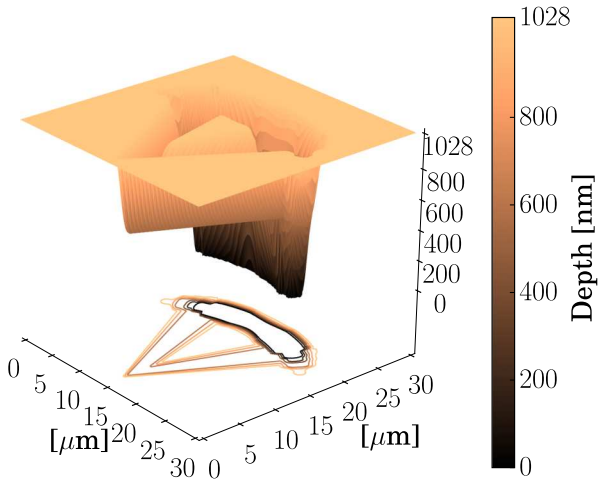

FIG. 6. Simulated depth profile of ablation of a 1028 nm thick parylene target after a single EUV laser pulse of 50 μJ energy. The innermost depth contour (at 0 depth) corresponds to the region where the target has been perforated.

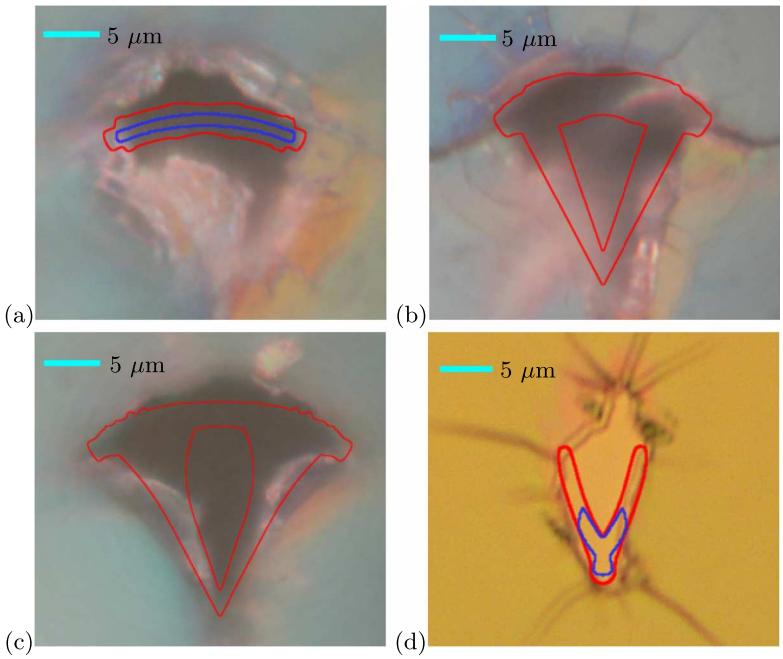

FIG. 7. Contours (red) of simulated perforation of parylene targets of 1028 nm thickness after (a) 1, (b) 2, (c) 30 shots. (d) Contours (red) for a 429 nm thick target after 1 shot. The targets were ablated at varying distances along the beam propagation axis, leading to different intensity profiles. Regions of perforation during a single laser pulse (blue), as determined by transmission measurements discussed in Section V.

the Fraunhofer diffraction form of Equation (3). In Cartesian coordinates, it can be solved efficiently by a 2-dimensional fast Fourier transform.

POLLUX simulations predict approximately a constant refractive index across the regions where the target has been penetrated by the laser beam, while the regions where the paryene remains solid are opaque to EUV radiation. Therefore, the target is assumed to act purely as a time-varying spatial filter for the focal intensity profile, as unablated material is opaque. We match the measured transmission by a weighted sum (to account for the pulse's Gaussian temporal profile) of Fraunhofer diffraction patterns through simulated perforation of the targets (as outlined in Sec. IV) in Figure 8. The transmission through a 429 nm thick target calculated in this way can be clearly matched

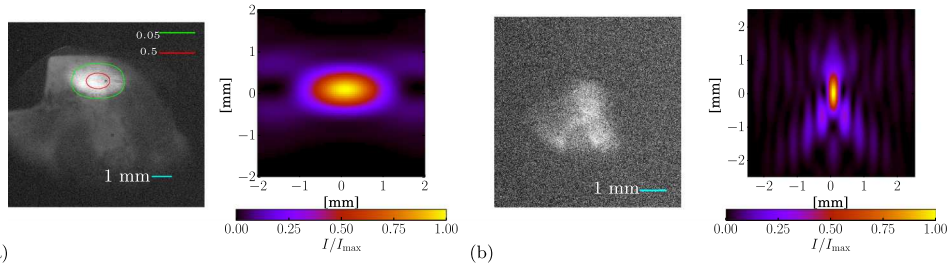

(a) (b)

FIG. 8. CCD images and diffraction simulations of single-shot transmission through parylene targets. (a) Transmission through targets of 429 nm thickness, with contours of constant intensity from simulations (as indicated) overlaid onto the CCD image. (b) Increased contrast CCD image of transmission through targets of 1028 nm thickness.

to the experimental measurement; constant intensity contours are overlaid on the CCD image to illustrate this. The 1028 nm thick foil absorbs a larger fraction of the laser pulse, leading to a lower signal-to-noise ratio. Nonetheless, the simulations predict a three-pronged structure in the transmission measurement as observed.

The intensity in the latter half of the pulse, when significant ablation has occurred, decreases with time and therefore the main contribution to the transmitted intensity is from the period shortly after the target becomes transmissive. The regions providing the dominant contribution to the transmitted intensity during a single shot are highlighted in Figures 7(a) and 7(d) for appropriate target thicknesses. Taking, for example, the final perforations as the spatial filter for the focused beam produces a poorer fit to the measured transmission; in the case of the 429 nm foil, this manifests as a change in the aspect ratio of the intensity contours. It is clear that shocks and other effects after the laser pulse have enlarged the laser crater.

VI. CONCLUSION

The feasibility of using a single pulse to create and diagnose a dense plasma has been demonstrated by imaging its transmission through a thin target. EUV laser pulses were focused by a tilted spherical multilayer mirror to intensities of up to 3×10^{10} W cm^{-2}. To simulate the resultant asymmetric intensity profile, we have adopted a wave optics approach, including multilayer mirror effects, which agrees with experiment. This focusing approach has produced a wide variation in intensities, whose ablation of solid foils has been matched by radiation-hydrodynamic simulations. The 2-dimensional (cylindrically symmetric) code `POLLUX` was used to simulate the fundamentally 3-dimensional ablation profiles, because of the low heat and momentum transfer perpendicular to the laser beam.

CCD images of this transmission are consistent with spatial filtering by the shape of the perforation made in the target. A more detailed calculation of the complex refractive index of the plasma during similar laser interactions would allow its spatial variations to be diagnosed.

ACKNOWLEDGMENTS

The UK authors acknowledge UK funding from AWE Plc. and the Engineering and Physical Science Research Council (Grant No. EP/J0194021). This work was supported by the U.S. Department of Energy, Office of Science, Basic Energy Sciences (BES), under award number DE-FG02-04ER15592.

[1] A. Caruso and R. Gratton, Plasma Phys. **10**, 867 (1968).
[2] B. C. Boland, F. E. Irons, and R. W. P. Mcwhirter, J. Phys. B: At. Mol. Phys. **1**, 1180 (1968).
[3] S. M. Vinko, U. Zastrau, S. Mazevet, J. Andreasson, S. Bajt, T. Burian, J. Chalupsky, H. N. Chapman, J. Cihelka, D. Doria, T. Döppner, S. Düsterer, T. Dzelzainis, R. R. Fäustlin, C. Fortmann, E. Förster, E. Galtier, S. H. Glenzer, S. Göde, G. Gregori, J. Hajdu, V. Hajkova, P. A. Heimann, R. Irsig, L. Juha, M. Jurek, J. Krzywinski, T. Laarmann, H. J. Lee, R. W. Lee, B. Li, K.-H. Meiwes-Broer, J. P. Mithen, B. Nagler, A. J. Nelson, A. Przystawik, R. Redmer, D. Riley, F. Rosmej, R. Sobierajski,

F. Tavella, R. Thiele, J. Tiggesbäumker, S. Toleikis, T. Tschentscher, L. Vysin, T. J. Whitcher, S. White, and J. S. Wark, Phys. Rev. Lett. **104**, 225001 (2010).
[4] A. J. Nelson, S. Toleikis, H. Chapman, S. Bajt, J. Krzywinski, J. Chalupsky, L. Juha, J. Cihelka, V. Hajkova, L. Vysin, T. Burian, M. Kozlova, R. R. Fäustlin, B. Nagler, S. M. Vinko, T. Whitcher, T. Dzelzainis, O. Renner, K. Saksl, A. R. Khorsand, P. A. Heimann, R. Sobierajski, D. Klinger, M. Jurek, J. Pelka, B. Iwan, J. Andreasson, N. Timneanu, M. Fajardo, J. S. Wark, D. Riley, T. Tschentscher, J. Hajdu, and R. W. Lee, Opt. Express **17**, 18271 (2009).
[5] J. Chalupsky, L. Juha, V. Hyjkovy, J. Cihelka, L. Vysin, J. Gautier, J. Hajdu, S. P. Hau-Riege, M. Jurek, J. Krzywinski, R. A. London, E. Papalazarou, J. B. Pelka, G. Rey, S. Sebban, R. Sobierajski, N. Stojanovic, K. Tiedtke, S. Toleikis, T. Tschentscher, C. Valentin, H. Wabnitz, and P. Zeitoun, Opt. Express **17**, 208 (2008).
[6] S. P. Hau-Riege, R. A. London, A. Graf, S. L. Baker, R. Soufli, R. Sobierajski, T. Burian, J. Chalupsky, L. Juha, J. Gaudin, J. Krzywinski, S. Moeller, M. Messerschmidt, J. Bozek, and C. Bostedt, Opt. Express **18**, 23933 (2010).
[7] R. W. Lee, S. J. Moon, H.-K. Chung, W. Rozmus, H. A. Baldis, G. Gregori, R. C. Cauble, O. L. Landen, J. S. Wark, A. Ng, S. J. Rose, C. L. Lewis, D. Riley, J.-C. Gauthier, and P. Audebert, J. Opt. Soc. Am. B **20**, 770 (2003).
[8] M. Fajardo, P. Zeitoun, and J.-C. Gauthier, Eur. Phys. J. D **29**, 69 (2004).
[9] M. Berrill, F. Brizuela, B. Langdon, H. Bravo, C. S. Menoni, and J. J. Rocca, J. Opt. Soc. Am. B **25**, B32 (2008).
[10] J. J. Rocca, V. N. Shlyaptsev, F. G. Tomasel, O. D. Cortazar, D. Hartshorn, and J. L. A. Chilla, Phys. Rev. Lett. **73**, 2192 (1994).
[11] B. R. Benware, A. Ozols, J. J. Rocca, I. A. Artioukov, V. V. Kondratenko, and A. V. Vinogradov, Opt. Lett. **24**, 1714 (1999).
[12] S. Heinbuch, M. Grisham, D. Martz, and J. J. Rocca, Opt. Express **13**, 4050 (2005).
[13] B. A. Reagan, K. A. Wernsing, A. H. Curtis, F. J. Furch, B. M. Luther, D. Patel, C. S. Menoni, and J. J. Rocca, Opt. Lett. **37**, 3624 (2012).
[14] H. Bravo, B. T. Szapiro, P. W. Wachulak, M. C. Marconi, W. Chao, E. H. Anderson, D. T. Attwood, C. S. Menoni, and J. J. Rocca, IEEE J. Sel. Top. Quantum Electron. **18**, 443 (2012).
[15] G. Vaschenko, A. Garcia Etxarri, C. S. Menoni, J. J. Rocca, O. Hemberg, S. Bloom, W. Chao, E. H. Anderson, D. T. Attwood, Y. Lu, and B. Parkinson, Opt. Lett. **31**, 3615 (2006).
[16] I. Kuznetsov, J. Filevich, F. Dong, M. Woolston, W. L. Chao, E. H. Anderson, E. R. Bernstein, D. C. Crick, J. J. Rocca, and C. S. Menoni, Nat. Commun. **6**, 6944 (2015).
[17] L. Juha, V. Hajkova, J. Chalupsky, V. Vorlicek, A. Ritucci, A. Reale, P. Zuppella, and M. Störmer, J. Appl. Phys. **105**, 093117 (2009).
[18] C. Liberatore, K. Mann, M. Mueller, L. Pina, J. Juha, L. Vysin, J. J. Rocca, A. Endo, and T. Mocek, Phys. Scr. **T161**, 014066 (2014).
[19] C. Spindloe (Scitech Precision Limited), private communication (2015).
[20] D. L. Windt, Comput. Phys. **12**, 360 (1998).
[21] J. L. A. Chilla and J. J. Rocca, J. Opt. Soc. Am. B **13**, 2841 (1996).
[22] E. Hecht, *Optics*, 3rd ed. (Addison Wesley, 1998).
[23] P. J. Davis and P. Rabinowitz, *Methods of Numerical Integration*, 2nd ed. (Academic Press, 1984).
[24] G. J. Pert, J. Plasma Phys. **41**, 263 (1989).
[25] A. K. Rossall, V. Aslanyan, and G. J. Tallents, Proc. SPIE **8849**, 884912 (2013).
[26] A. K. Rossall, V. Aslanyan, G. J. Tallents, I. Kuznetsov, J. J. Rocca, and C. S. Menoni, Phys. Rev. Appl. **3**, 064013 (2015).